The International Journal of Engineering and Science (IJES)
|| Volume || 8 || Issue || 10 Series II || Pages || PP 01-14 || 2019 ||
ISSN (e): 2319 – 1813 ISSN (p): 23-19 – 1805

Operating Limits of Railway Lock Stretcher Bar Movements via Multiaxial Analysis

Wahid Ludeen[1, 2], Hassan Hemida[2] and Edward Stewart[2]
[1]*Atkins, London, United Kingdom;*
[2]*School of Engineering, University of Birmingham, Birmingham, United Kingdom*
Corresponding Author: Wahid Ludeen

----------***ABSTRACT:***----------
A lock stretcher bar (LSB) is an important component of the switching mechanism in a railway switch and crossing layout system, and is thought to have been the main cause of failure in several railway accidents.This study provides an improved understanding of the failure characteristics of railway switch LSB in operation using computational models. Finite element analysis software is used to simulate multiaxial deformation of a standard lock stretcher bar used in some UK switches and crossings. The model is successfully validated using experimental methods. Safe deflection limits have been obtained for multiple displacement directions which collectively create a three-dimensional operating safety envelope.The findings show that as the direction at which the LSB is deformed becomes increasingly oblique, the yield displacement gradually decreases, reaching a sharp minimum midway between any given principal axes. Allowable deformations are smaller than those assumed in previous research for most deflection directions. Since LSB are unlikely to deform in only one direction about the principal axes, the biaxial envelope must be used when specifying the suitability of LSB in the switching panel.

Keywords*: lock stretcher bar, switch and crossing, biaxial deformation, safety envelope, yield displacement*

Date of Submission: 20-10-2019 Date of acceptance: 03-11-2019

I. INTRODUCTION

Switch and crossings (S&C) allow a train to move from one railway track to another, enabling a multi-lined and interconnected rail network. Switches and crossings make up less than 5% of track miles in the UK, yet over 17.4% of the annual maintenance budget is spent on them [1]. The relative intricacy and dynamic nature of S&Cs makes them points of vulnerability and weakness in a rail network, this results in a higher requirement for monitoring and maintenance than for plain track.

The need to improve reliability and reduce life cycle costs of S&Cs is becoming increasingly important. Predictions forecast ever increasing reliance on rail as a mode of transport and this combined with higher passenger numbers could likely result in higher train numbers, line speeds and axial loads on the track. All of these things contribute further to the risk of S&C failure. Growing automation of transport systems, including railway networks, increases the need to improve reliability and our understanding of when and where failures in the physical infrastructure are likely to occur. Failures in the network cause delays and in severe cases may lead to catastrophic accidents and fatalities. S&Cs are linked with the largest proportion of reported track faults [2]. A lock stretcher bar (LSB) is a component of the switching panel in an S&C layout and is thought to have been the main cause of failure in several railway accidents [3, 4]. Further understanding the component characteristics and failure processes in S&Cs allows improvements in dependability and contributes to the reliability of the railway network.

This paper presents the findings of an investigation into the failure characteristics of the lock stretcher bar in operation via three-dimensional finite element analysis and aims to provide an improved understanding of its operational behaviour when exposed to biaxial deformations. In previous work, by interpolation, using uniaxial deformation data it has been assumed that the safety envelope of a lock stretcher bar is linear when subjected to biaxial deformations.

1. Pre-processing

Switch and crossing, often referred to as a turnout (Figures 1 and 2), are junctions in a rail network which facilitate the movement of a railway vehicle from one railway track to another. S&Cs are usually considered as three separate units, these are known as panels. The switching panel is the first point of interaction between the vehicle and the S&C junction. Its role is to enable a smooth entry into the switch in the nominated direction, either by guiding the train to the diverging track or allowing it to continue traveling in the “normal”

direction. The crossing panel is then followed by the closure panel where the final stages of the transition from the through track to the diverging track are made.

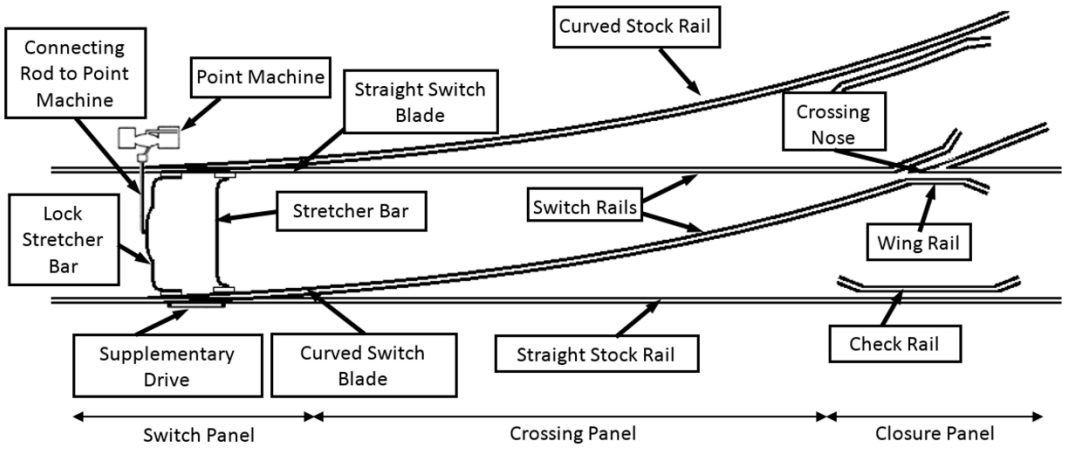

Figure 1. Layout of switch and crossing.

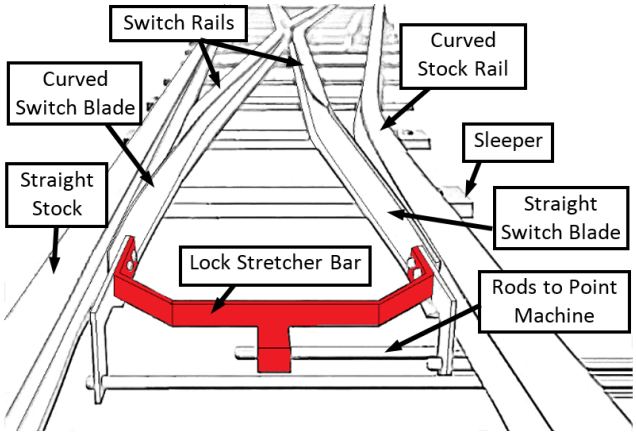

Figure 2. Switch panel layout.

The movements in a switch are driven by a point machine, which is a remotely controlled electronic component. The point machine transfers either a pulling or pushing lateral force to the lock stretcher bar moving the switch blades and rails into the designated position. The switch blades lie between the straight and curved stock rails, and are connected to each other via the lock stretcher bar which maintains a defined horizontal separation and therefore ensures the blades move simultaneously as a coupled pair. When a switch is moved, one of the blades comes to rest on either the straight stock rail or the curved stock rail, whilst the other blade is moved away from the opposite conjugate stock rail. A clearance is created for the train's wheel flanges where there is a separation between the switch blade and stock rail. The resulting arrangement dictates the train's direction of travel, as illustrated in Figure 3.

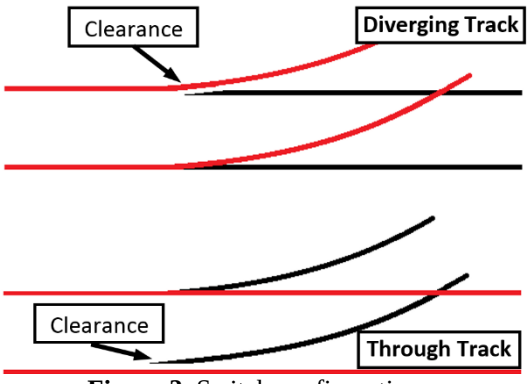

Figure 3. Switch configurations.

It is important the switch blades move simultaneously, allowing for a constant track gauge between the rails. The distance separating the left and right rail on a track must always be constant, including in the S&C panels. The number of stretcher bars used in a switch is dependent upon the curvature of the turnout and therefore its length. A longer switch may also have supplementary drives which aid the movement of the switch rails along its length. The length of a switch dictates the rate at which the switch induces a change in travelling direction and thus the maximum speed at which train is expected to pass over the switch [5].

Steel rails are flat-bottomed and are supported on sleepers, which are laid on stones known as ballast. The rail fastening system for the stock rails is fixed, whereas on switch rails, slide chairs on the sleepers allow for lateral movement thus enabling the switch rails to slide side to side when the switch is moved. The point machine must exert a force on the lock stretcher bar overcoming both the frictional resistance presented by the slide chairs and the natural flexural rigidity of the switch rail. Switch rails are fixed at the crossing and free to move laterally at the switch toe. The point machine is connected to the LSB via a connecting rod. In addition to moving the switch, the point machine holds the switch blades in their final position via a locking mechanism. A detection mechanism (commonly electromechanical) uses detection rods like those shown in Figure 2 to monitor the position of the switch rail thus ensuring full contact with the stock rails before a signal can be given to the train for safe passage over the switch.

Lock stretcher bars are usually flat bars of steel bent into shape and are connected to the web of switch blades with two bolts at each connection. The shape and geometric properties of the stretcher bar is based on a compromise between the need for a stiff bar which moves rigidly and holds the switch blades in position and one that is able to flex moderately, absorbing deflections passed to the bar and its connections while in operation. Insulating jackets are placed on either side of the LSB at the bolted connections. This electrically insulates the LSB from the switch blades such that it does not interfere with the signalling system. The LSB connects the two switch blades, ensuring they move together and are held firmly against the stock rails when the point machine's locking mechanism has been engaged. It also adds additional lateral

stability to the relatively slender and open-ended switch blades ensuring they remain upright.

Failure of the LSB can lead to variation in the spacing of the switch rails or an insecure contact between a switch and a stock rail pair. Both of these effects can ultimately be causes of derailment.

1.1. Structural Performance of S&Cs and its Components

A switch and crossing is subjected to varying high impact dynamic loads. The individual components found in the switching panel, such as the lock stretcher bar, which has a dynamic role itself, must be resilient against these secondary loads. If a lock stretcher bar were to fail, either by deforming out of shape, fracturing or disengaging at either of its connecting points, its role in the switching panel would be compromised and safety put at risk. Wheel-rail contact induces vertical, lateral, and axial deformations in the track which are then transferred to the lock stretcher bar. This is in addition to the stresses imposed on the lock stretcher bar by the point machine or during assembly via its bolted connections. Vertical forces are a result of a train's axial load. Lateral forces are induced as the train negotiates a curve, and longitudinal forces occur as a result of temperature variations, traction, and acceleration/deceleration of the train. Rail vehicles are rapidly accelerated to change direction at turnouts. In conjunction with high travelling speeds, impact loads of high frequency are imposed on the rail track at switches and crossings, which travel to the lock stretcher bar. The forces imposed on rails in turnouts are largely dependent on the speed and mass of the vehicle. Aniołek and Herian [6] determined the vertical and lateral forces at points of wheel-rail contact by numerically modelling the interaction. In this instance, a vertical force of 172 kN is observed at each contact point when the vehicle is travelling at 60 km/h, and there is a decrease in force of 30% when the travelling speed is reduced to 20 km/h. Lateral forces are limited to a maximum of 34 kN at all travelling speeds. This limit is imposed by the provision of safety wings and check rails which provide lateral support.

Once the switch has been moved into its designated position, the locking mechanism in the point machine continually exerts a force on the stretcher bar, holding it in position as the train passes over the switch. The stabilising force of the point machine must be strong enough to resist lateral movements of up to 5 mm at the switch blade toes induced by the interaction between train and track [7].

The geometric and cross-sectional properties of the lock stretcher bar determine its flexural rigidity and deflection limits in different directions. Lock stretcher bars are usually made of steel. The grade of steel used for switch and crossing components varies in different countries. The UK uses a grade of R260, however, a grade of R350HT (350 hardness; heat treated) or higher is specified as a national guideline in most European countries [8]; the higher grade provides increased resistance to wear and rolling contact fatigue. A lock stretcher bar's chemical contents may be varied by alloying elements which enhance its structural characteristics, such as its hardness, toughness, and ductility. Nevertheless, the general behavioural patterns do not vary significantly given the short operational movement of lock stretcher bars; a typical stress-strain graph for steel is shown in Figure 4. Since the effective operation of the lock stretcher bars is sensitive to its geometrical shape, any permanent

changes can be dangerous rendering it ineffective in correctly separating and stabilising the switch blades. It has been reported that lock stretcher bars are most likely to reach their plastic limit at the first bolt hole, i.e. the one closest to the switch blade toe [9]. Once the steel has been stressed past its yielding point, the LSB starts to deform plastically and may no longer maintain the design separation between the two switch blades. Deflections up to the yield stress are reversible and deemed safe, this assumption will be the basis of any safety envelopes presented in this study.

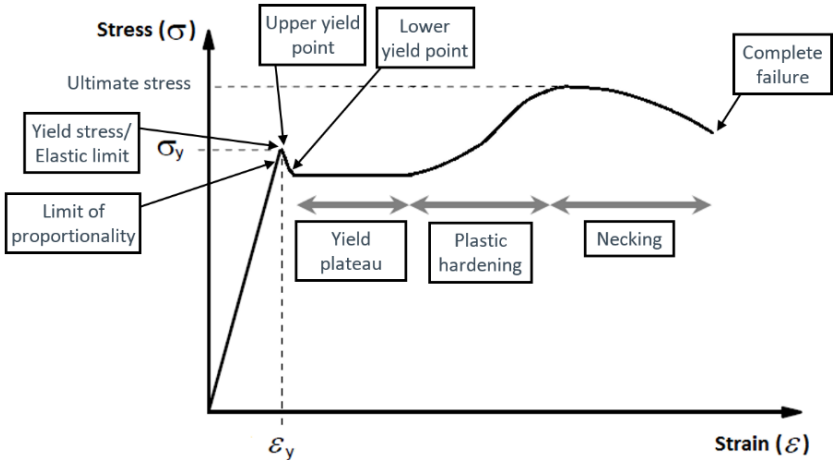

Figure 4. Typical stress-strain curve for steel.

It is important that the lock stretcher bar does not enter a state of plastic deformation at any time throughout its lifetime. The role of the LSB is strictly shape dependent – if it were to either stretch, shrink or bend permanently, the potential for an incomplete switching operation is increased. Understanding the structural performance of the LSB and its 'safe' operating conditions is vital to reducing the risk of failure in the switching panel. Licciardello et al. [10] investigated the displacement of railway switching panels in field tests with both freight and passenger trains and noted the maximum lateral displacement of the switch blade as -5 mm, and the maximum vertical displacement as -2.5 mm (negative values indicate downwards deformation). These deformations seen by the switch blade are transferred to the lock stretcher bar directly via the fixed connection between the two elements and must be accounted for when specifying the structural performance requirements of the lock stretcher bar. A lock stretcher bar must have a design capacity which notably exceeds its characteristic requirements in operation.

From an economic and safety standpoint, there is a strong need to develop our understanding of S&C component failures. Switches and crossings make up less than 5% of track miles in the UK, yet over 17.4% of the annual maintenance budget is spent on them [1]. There are over 20,000 S&C units across the UK's 21,000 mile rail network. Ma et al. [11] identified the highest level of specific risk of failure in a rail network is found in switches. The ability to predict failures and the operating lifetime of individual switching components supports the comprehensive cost-benefit analysis of improving the design of and replacing existing lock stretcher bars across the rail network. Understanding the condition and degradation modes for a component allows greater management and scheduling of inspection and routine maintenance work. Additionally, there is a reduced likelihood of the railway track entering a hazardous state and thus needing emergency maintenance which can be particularly disruptive.

Rail accident history can attest to the need to improve understanding of individual switching panel components and their failures. The failure of lock stretcher bars has been the primary cause of derailment of some trains in the past, namely at Potters Bar in 2002 and Grayrigg in 2007. In both cases a failure to adequately inspect and identify a need for maintenance work lead to the stretcher bars and their accompanying connecting components to critically degrade unnoticed. In the case of Grayrigg, RAIB [3] reported all nine coaches of the train derailed the track while it travelled over the failing switch at a legal speed of 95mph in Lambrigg, near Grayrigg in Cumbria. One passenger was killed and many injured. The lock stretcher bar and all three stretcher bars were found to have failed, each contributing to the accident. It is thought the right-hand switch rail was locked to the diverging stock rail while the LSB's left hand fasteners had failed resulting in the stretcher bar and detecting rod detaching from the switch blade. Consequently, the blade flexed, closing the minimum 50 mm flange clearance to approximately 10-20 mm without detection. This arrangement meant both switch blades were aligned adjacent to their pairing stock rail and so the train car's wheels were forced to move in opposite directions towards each other causing a derailment. Similarly, at Potters Bar, one of the LSB's bolted

connections had failed resulting in the decoupling of the switch blades and hence the derailment of the rear end of the train causing 7 deaths [4].

1.2. Failure Mechanisms of Lock Stretcher Bars

Comparatively few research papers have been published targeting the interaction between railway vehicles and track in S&Cs relative to normal straight track, and even fewer studying the different components in the switching panel despite their relative complexity and dynamic role making them points of vulnerability and weakness in a rail network. However, some noteworthy work in field has been carried out including that of Ma et al. [11] who identified the highest level of specific risk in a rail network is in the switching panel.

The majority of research published regarding the structural analysis of switches and crossings has been conducted by means of either analytical modelling or experimentation. The dynamic interaction between the train and railway turnouts was studied by Kassa and Nielsen [12]. Wheel-rail contact was investigated experimentally, detecting lateral and vertical contact forces by placing strain gauges on the train wheel discs. It was concluded that both lateral and vertical contact forces are highest in the switching panel when the train is diverging from the main route, these forces are further elevated at higher traveling speeds and axle loads. Lateral and vertical loads were not significantly influenced by changes in train speed on the through route. Their findings were validated by numerical simulations. Pålsson and Nielsen [11] also studied wheel-rail interaction and damages in S&Cs and found results which were in agreement with those of Kassa and Nielsen.

Mathematical models of train and S&C interactions by Alfi and Bruni [14] investigated wheel-rail impact at the point of transfer from one track to another i.e. at the switch blade toes and at the crossing nose. As a wheel transitions from stock rail to the switch blade, the contact force is significantly elevated when the wheel is in contact with both rails at the point of discontinuity. The largest impact force occurs at the crossing nose, producing significant dynamic lateral and vertical reaction forces on the wheel and track, largely due to the discontinuity in rail profile presented at the crossing panel. Slippages between the wheel-rail interfaces at the crossing nose increase abrasive wear and fatigue wear, which is partly combated by the installation of check rails on some crossing panels. These findings are in agreement with those of Pletz et al. [15] and Pålsson and Nielsen [13] who too studied wheel-rail interactions in S&Cs investigating the influence of wheel profile, axle load and train speed. Eck et al. [16] found similar results, investigating the influence of steel grades used in S&C rails. A track geometry which facilitates a non-smooth transition accelerates degradation regardless of track material [17].

Nicklisch et al. [2] investigated geometry and stiffness optimisation for S&Cs and found the installation of elastic rail pads reduced support stiffness thus reducing wheel-rail impact loads considerably, particularly on diverging track at high speeds. Due to its setup and varying geometry, switch and crossing junctions have variable support stiffness. Load distribution and contact pressures differ at different points along the switch, and as a result localised track settlements are likely to accumulate [18]. Vertical irregularities and track movements are expected to accelerate the deterioration of individual switching components, exposing them to operating conditions which they have not been designed for. For the purpose of this study it has been assumed variable support stiffness and their effects can be ignored.

Hemida et al. [9] who investigated the performance of lock stretcher bars, simulated via finite element (FE) analysis different operational and assembly conditions. Loads and deformations were studied on an isolated LSB from a short, shallow depth switch. A safety envelope was obtained and successfully validated with experimental measurements, establishing the maximum serviceable deflections the LSB could tolerate before failing. However, displacement limits were identified in just the orthogonal directions per simulation run, and hence, the full safety envelope was assumed based on linear interpolation between the few deformation directions investigated (see Figure 5). This paper aims to verify, or otherwise, the validity of the linear interpolation assumption made by Hemida et al.

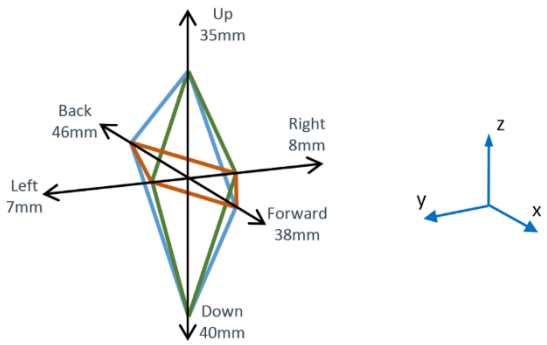

Figure 5. Assumed safety envelope of LSB based on nodal data, adapted from [9].

In practice, lock stretcher bars are unlikely to deflect in only one orthogonal direction during most operational scenarios. Simulating the application of a combination of loading scenarios, by coupling different orthogonal deformation directions, will yield more accurate and representative structural characteristics of a lock stretcher bar in operation. As an example, a lock stretcher bar may be required to resist the locking force imposed by the point machine in combination with the vertical displacements induced by the weight of a rail vehicle. In this scenario the lock stretcher bar is simultaneously exposed to both a lateral and vertical deformations, hence its resultant deformation is biaxial and out of plane from the principal x, y or z planes.

Montesano and Singh [19] noted higher stresses are shown when members with parallelogram shaped cross sections are stressed biaxially. Structural members are usually required to resist bending moments and transverse forces about axes parallel to their outer faces. By altering the direction in which the load is applied, the member's second moment of inertia is reduced and the eccentricity between the neutral axis and furthest cross-sectional perpendicular edge is maximised. Therefore, the member reaches yield stress much sooner. The findings of Montesano and Singh [19] are consistent with those of Baptista [20].

2. Pre-processing

The height of the LSB is generally 60 mm but reduces to 56 mm along the length of the insulating jacket, which also has a height of 56 mm. It is 15 mm thick along its entire length. The boundary conditions of the model are idealistically consistent with that of LSB in operation - one end is fixed (as shown in Figure 6) while the other end is subjected to displacements of 50 mm in 62 different deflection directions.

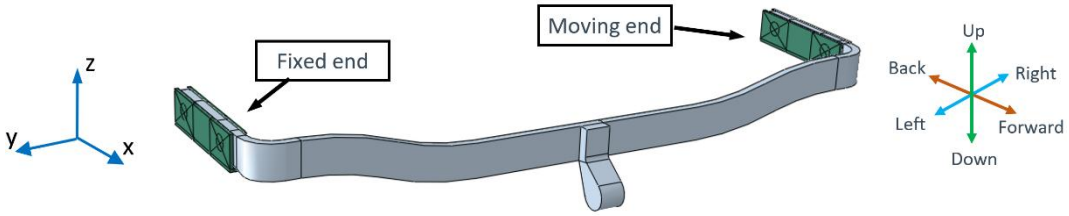

Figure 6. Lock stretcher bar model with ideal insulating jacket.

The finite element analysis package ABAQUS is used to model and simulate the lock stretcher bar in operation. The operating conditions are simulated using general static and dynamic explicit solvers. Computational modelling and simulations provide a convenient and safe tool for reproducing the behaviour of a physical system; it may be favoured over experimental investigations which are vulnerable to real-world sources of error and variability in both setup and outcome. However, it should be noted that computational modelling methods are not always strictly representative of real-world conditions since notable simplifications are needed in most cases.

Finite element analysis requires the model to be divided into small 'finite' elements known as mathematical regions which, as part of the analysis process, are considered as separate structural elements. Consequently, the LSB is not modelled as one continuous member as is ideally required, instead a mesh of nodes and elements are created which collectively create a structural matrix for which the FE solver computes the analysis. The finite element model's (FEM) global mesh size is set to 5 mm creating a total of 26,968 nodes and 17,907 individual hexahedral elements, as illustrated in Figure 7. A stable solution which accurately models the propagation of high frequency waves though the LSB must have a time step that is smaller than the time step limit. The time step limit is automatically calculated and is a function of the material's density and its mesh size. For this problem the stable time step is very small and therefore divides the analysis into millions of increments.

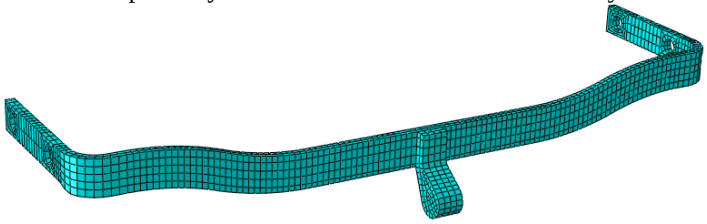

Figure 7. Lock stretcher bar model mesh of elements.

The lock stretcher bar is subjected to a displacement of 50 mm over a period of 6 seconds per simulation. In ABAQUS, a series of 'time steps' solve for stresses statically by determining the LSB's deformation periodically, simulating the dynamic process as a series of thousands of steps. In theory this presents a source of inaccuracy since inertial forces are mostly eliminated from the process, however, the time

steps are suitably small and therefore render the influence of inertial forces negligible. A reasonable assumption can be made stating that the simulation behaves dynamically. The explicit solver uses the central difference method to calculate the nodal acceleration(u) at the beginning of each time increment (t) based on the dynamic equilibrium Equation 1 [21].

$$\ddot{u}|_{(t)} = (M)^{-1}(P - I)|_{(t)} \quad (1)$$

Where (M) is the nodal mass matrix, (P) is the vector of the externally applied forces and (I) is the vector of internal element forces [21]. The acceleration at any nodal point is determined through its mass and resultant force. The velocities (ü) and displacements (u) are advanced "explicitly" through each time increment (Δt), as shown in Equations 2 and 3.

$$\dot{u}|_{(t+\Delta t/2)} = \dot{u}|_{(t-\Delta t/2)} + \frac{\Delta t|_{(t+\Delta t)} + \Delta t|_{(\Delta t)}}{2} \ddot{u}|_{(t)} \quad (2)$$

$$u|_{(t+\Delta t)} = u|_{(t)} + \Delta t|_{(t+\Delta t)} \dot{u}|_{(t+\Delta t/2)} \quad (3)$$

The lock stretcher bar is modelled with BS EN 10025 Grade S355JO steel for which the stress-strain curve has been produced in the Metallurgy and Materials laboratories at the University of Birmingham through axial stress tests. As part of the analysis process ABAQUS requires true stress-strain values as a parameter for the model's material. True engineering stress-strain accounts for the shrinking cross-sectional area of an element as it is elongated. Engineering stress-strain values obtained in the laboratory have been converted to true stress-strain values using Equations 4 and 5. Figure 8 shows the engineering and true stress-strain graphs for the LSB respectively. The yield stress for this LSB is 260 MPa.

$$\sigma_{true} = \sigma_{eng}(1 + \varepsilon_{eng}) \quad (4)$$

$$\varepsilon_{true} = ln(1 + \varepsilon_{eng}) \quad (5)$$

Where σ_{true} and ε_{true} are the true stress and strain respectively.

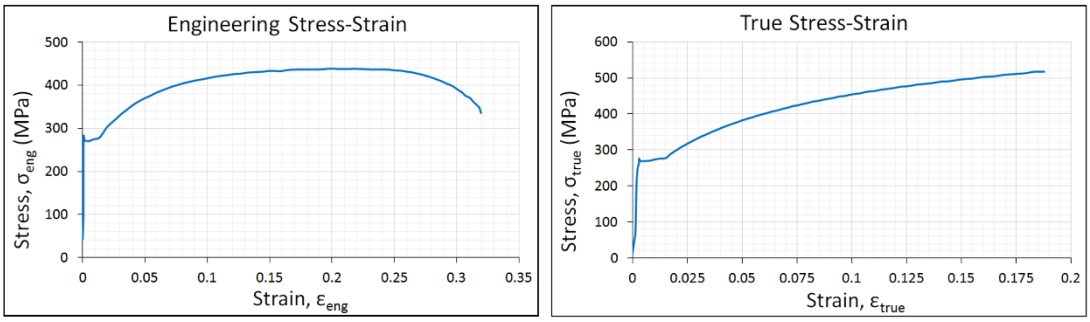

Figure 8. Engineering and true stress-strain graphs for the LSB.

In a railway switch an insulating jacket is placed on either side of the bolted section of the lock stretcher bar in order to electrically insulate it from the switch blades. Abearing pressure is exerted on the relatively soft insulating jacket during assembly via the bolted connections. This causes the jacket to deform as shown in Figure 9(a). Stresses on the LSB are then concentrated around the bolt holes. The deformed insulating jacket case is representative of most insulating jackets found in switches across the UK. An 'ideal jacket' can be created by placing a rigid material between the bolts' washers and the insulating jacket, preventing stress concentrations [9]. For the purpose of this study only one model variation is studied - an ideal insulating jacket.

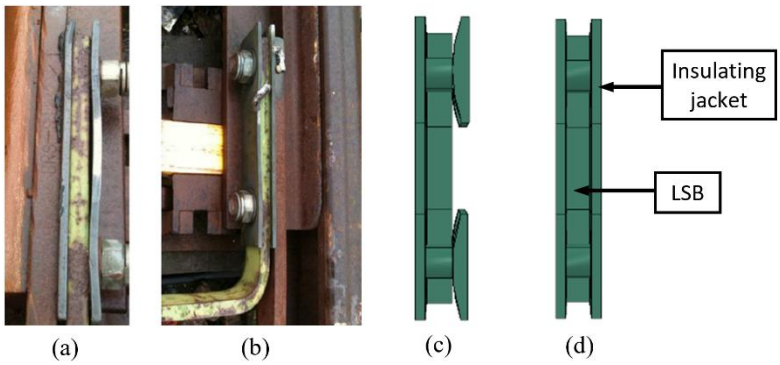

Figure 9. Insulating jacket assembly and model. Deformed (a,c), ideal (b,d).

The boundary condition of the moving end of the LSB is altered for each simulation/deflection direction. A biaxial movement is produced by simultaneously deflecting the LSB in two directions. A number of increments are achieved by altering the magnitude of the respective orthogonal deflection components. For example, to achieve a deflection of 45° between the Up and Right directions, a positive movement of 50 mm in the z-direction is coupled with a 50 mm negative movement in the y-direction, as per the axes shown in Figure 6. The deflection directions are made increasingly oblique relative to the principal orthogonal axes (x, y and z axis as per Figure 6) through a number of increments and a yield displacement reading is determined for each. The resulting output is a series of displacement limits which collectively can be used to generate the safety envelope of the LSB.

ABAQUS incrementally computes the deformation of the LSB and is able to identify the first instance at which any given element reaches and surpasses its yield stress. The deflection of the LSB at this point is the yield displacement for the given displacement direction. This concept is known as von Mises stress and relates to the distortion of the material. ABAQUS monitors the effective stress of all mesh elements and continually compares them to the yield stress assigned to the material. A von Mises stress that is larger than the yield stress indicates an element within the model has yielded. The displacement at which the lock stretcher bar first reaches its yield stress is recorded for each of the 62 displacement directions. This data is then plotted graphically to produce a safety envelope. This envelope represents the allowable deflection limits of the LSB before it enters a state in which it is plastically deforming and therefore causing a permanent change to the shape of the LSB.

3. Model Validation

The ABAQUS model is validated against a physical test specimen for which the physical parameters and operating conditions are replicated. As part of the experimental setup a hydraulic jack applies displacements to one end of a lock stretcher bar while the other end is fixed to a stock rail; these conditions imitate those of the FEA model. Strain gauges are placed at three locations on the surface of the LSB as shown in Figure 10. This experiment was conducted at the Birmingham Centre for Railway Research and Education at the University of Birmingham.

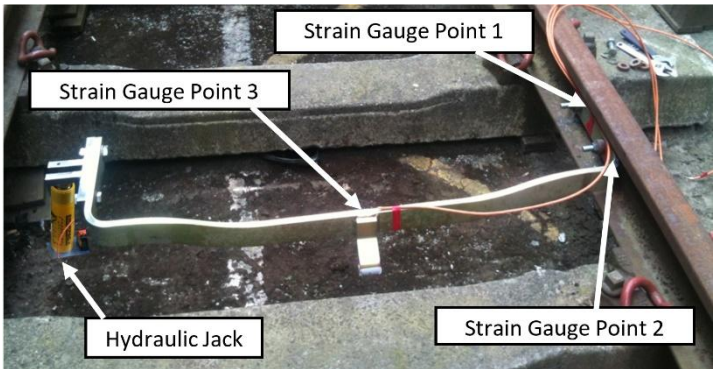

Figure 10. Experimental setup.

The force-displacement response shown in Figure 11 indicates that there is agreement between the experimental setup and the FEA model. The experiment was conducted three times demonstrating repeatability and during which force, displacement and strain gauge readings were recorded for the upward and downward displacement directions. There is a difference in the rate at which strain is applied to the LSB in the FE model and the experimental setup which may have caused the small difference between the two data sets (discussed further below). Nonetheless, the force-displacement results between the two data sets show strong agreement. It is worth noting the ABAQUS model assumes homogeneity of material properties and precise geometrical dimensions of the LSB; this may not be true for the specimen used as part of the experiment and so a small difference in the force-displacement curve is expected. Additionally, the physical condition and operational history of the LSB is unknown; time dependant changes in the structural properties of the LSB are therefore unaccounted for, further highlighting the significance of the idealistic-performing ABAQUS model.

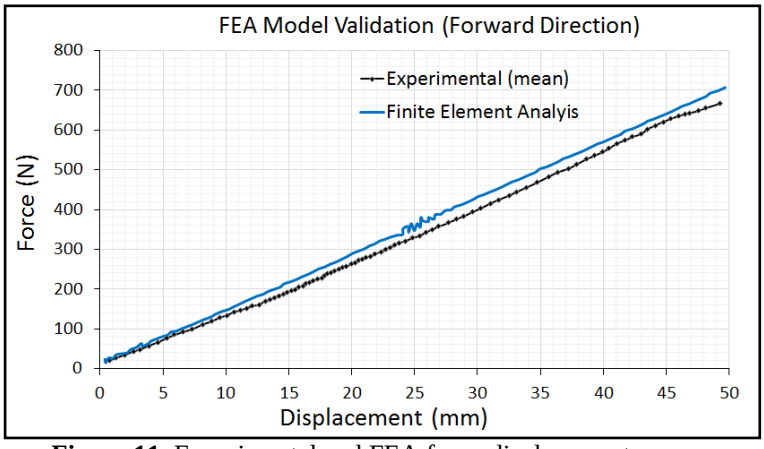

Figure 11. Experimental and FEA force-displacement curves.

A comparison between the readings obtained from the strain gauges and the strains observed in the FEA model show strong agreement. Strain readings are taken from points in the ABAQUS model which mirror the location of the strain gauges in the experimental setup (Figure 10). The strain-displacement curve at point 1, shown in Figure 12, shows a strong correlation. The level of agreement is similar at the other two gauge points. The higher frequency components of the experimental result, and the small differences observed between the two data sets, are representative of experimental noise in this kind of measurement.

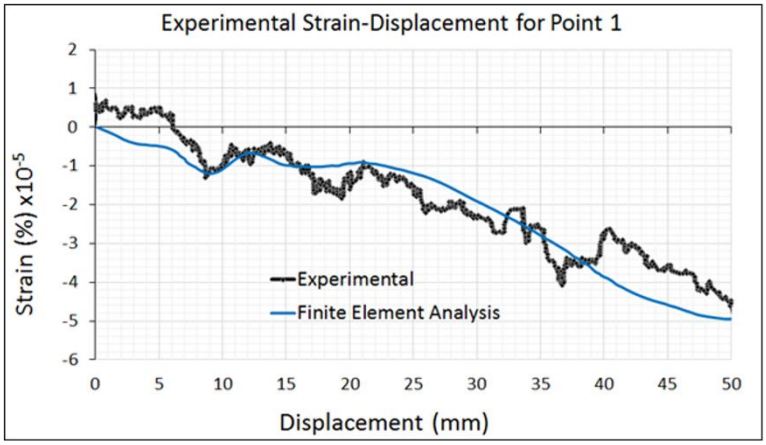

Figure 12. Strain-Displacement curves for strain gauge point 1.

II. RESULTS

This chapter presents and discusses the results of computational simulations carried out based on the methodology described in Chapter 3. A safety envelope is created based on the yield displacement values for each displacement direction simulated. The sections that follow provide critical analysis and discussion of the data obtained in this study, including an analytical justification for the structural behaviour observed.

2.1 Safety Envelope

The performance of the LSB has been investigated in a total of 62 deformation directions for which the yield displacement values are illustrated in Figures 13 and 14. Figure 13 illustrates the three-dimensional safety envelope obtained, Figure 14 presents plotted yield displacements obtained about the three deformation planes. Figures 14 (b), (d) and (f) illustrate the 62 deflection directions in which the LSB was investigated. The data obtained is consistent with that of Hemida et al. [9] i.e. the uniaxial yield displacement values (Up, Down, Left, Right, Back and Forward) match those of Hemida et al., therefore the two data sets are directly comparable. Figures 14 (a), (c) and (e) present a comparison between the previously assumed linear safety envelopes (old envelope) and those obtained in this study (new envelope).

Simulations are undertaken in every quadrant, but a greater number of biaxial smaller increments were simulated in the Up-Right and Up-Back quadrants. This leads to a higher level of detail in the safety envelope for those quadrants, as shown in Figures 14 (a) and (c).

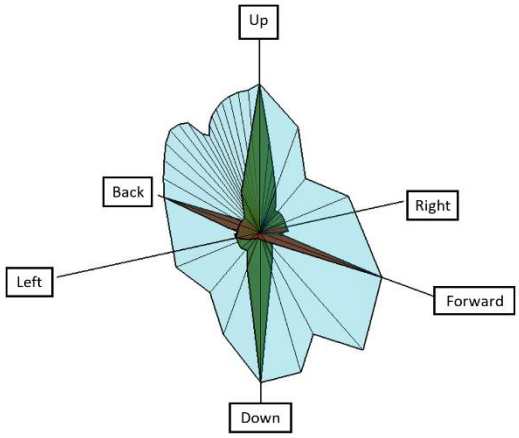

Figure 13. Safety envelope – 3D visualisation.

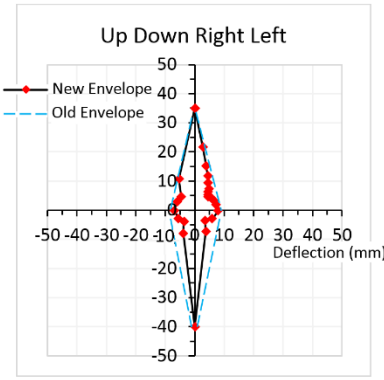

(a) Up Down Right Left envelope.

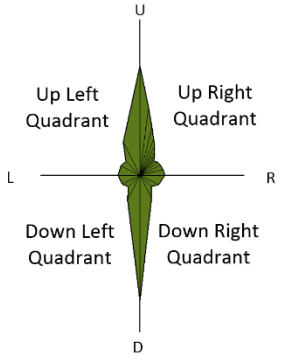

(b) Up Down Right Left displacements.

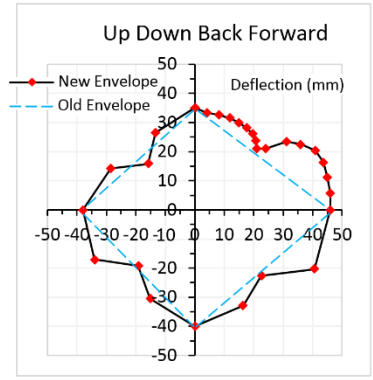

(c) Up Down Back Forward envelope.

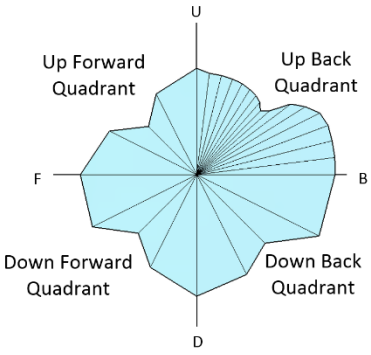

(d) Up Down Back Forward displacements.

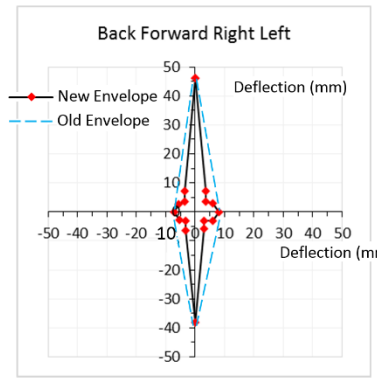

(e) Back Forward Right Left envelope.

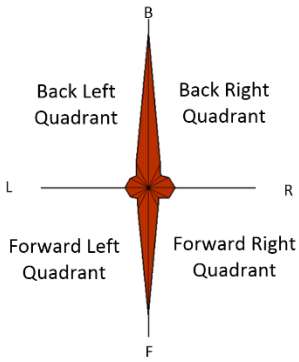

(f) Back Forward Right Left displacements.

Figure 14. Yield displacement results.

The safety envelopes show a non-linear relationship in each quadrant, thereby suggesting that the linear assumptions made by Hemida et al. [9] are in fact incorrect. A maximum allowable deflection is observed when the LSB is loaded uniaxially. As the deflection direction converges to halfway between the two principal axes, the displacement required to cause the LSB to yield gradually decreases, reaching a sharp minimum midway between the given principal axes. This pattern is observed for all quadrants about all the principal planes of deflection.

All biaxial yield deformations lie within the assumed safety envelope of Hemida et al. [9] for Figures 14 (a) and (e). Therefore, the LSB appears to be more sensitive to plastic displacements about these two deformation planes than previously assumed. However, for Figure 14 (c) almost all of the points lie outside the assumed linear envelope and so the LSB appears to be safer than previously thought about this plane.

2.2 Biaxial Deformation

A representative model can be used to explain the phenomenon seen in the results. Structural members are usually required to resist bending moments about axes parallel to their outer faces, as illustrated in Figures 15(b) and (c); moments about the principal X and Y axes are parallel to the edges of the rectangular cross section. Figures 15(b), (c) illustrate the application of bending moments about the principal axes and Figure 15(d) illustrates bending moments applied about two principal axes simultaneously, creating a resultant moment, M. The accompanying neutral axes and eccentricities of the uniaxial and biaxial scenarios are shown. An object with a parallelogram shaped cross section subject to biaxial transverse deflections will reach its yield stress sooner than if it were to be deflected uniaxially; a larger eccentricity taken between the neutral axis and the adjacent perpendicular point at the cross-sectional perimeter causes larger internal stresses and therefore yields sooner.

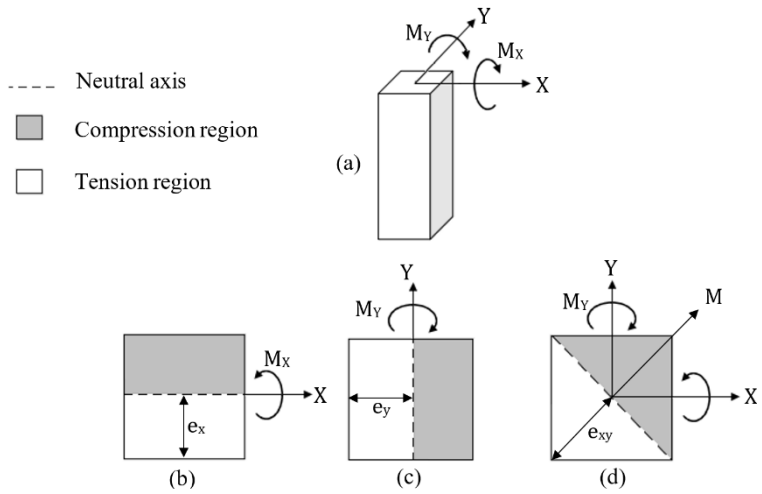

Figure 15. Biaxial bending of an element, (a) 3D view, (b) About X-axis, (c) About Y-axis, (d) Biaxial.

The eccentricity e_{xy} is greater than both ex and $e_y$therefore the biaxial scenario will reach higher internal stresses (at the corners of the cross section in the tension region) at smaller moments and deformations. The link between eccentricity and internal stresses can explain the patterns observed in the behaviour of the LSB and its safety envelope. The cross section of the LSB is rectangular along its entire length. As can be observed in the safety envelopes, a deflection direction that is midway between two orthogonal directions yields at the shortest deformations, the respective eccentricity of the cross section is highest in this displacement direction.

2.3 Analytical Model

The biaxial response of the LSB can be explained via an analytical model. The representative model represented in Figure 16 is fixed at one end and free to move at the other end, and has a rectangular cross-section. The deflection direction is parallel to the direction at which the load is applied.

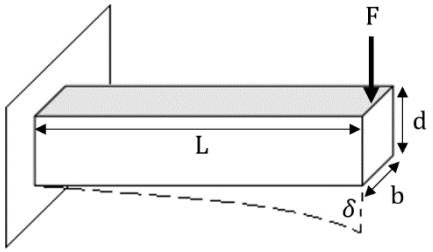

Figure 16. Representative cantilever beam (uniaxial deformation).

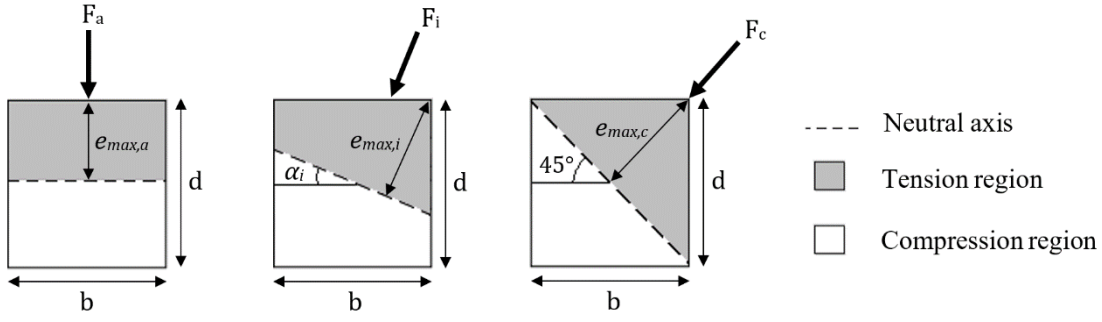

Figure 17. Uniaxial and biaxial response of representative cross-section, (a) Uniaxial deformation, α = 0 (b) Biaxial deformation, α = α (c) Biaxial deformation, α = 45°.

The relationship between the transverse load, F, for a cantilever beam and its deflection at the free end, δ, for both uniaxial and biaxial systems is:

$$F = \frac{3EI}{L^3}\delta \tag{6}$$

Where E is the elastic modulus of the member, and I is the moment of inertia:

$$I = \frac{bd}{12}(d^2\,cos^2\,\alpha + b^2\,sin^2\,\alpha) \tag{7}$$

Combining Equations 6 and 7 yields the following:

$$F = \frac{Ebd}{4L^3}(d^2\,cos^2\,\alpha + b^2\,sin^2\,\alpha)\delta \tag{8}$$

The flexural stress of the cross section is as follows, where M is the moment produced by the force F at a distance of L from the fixed end:

$$\sigma = \frac{Me_{max\,,i}}{I} = \frac{FLe_{max\,,i}}{I} \tag{9}$$

Substituting Equations 7 and 8 into Equation 9 yields the following:

$$\sigma = \frac{Ebd}{4L^3}(d^2\,cos^2\,\alpha + b^2\,\sin^2\,\alpha)\delta\,\frac{\mathrm{Le_{max\,,i}}}{\frac{bd}{12}(d^2\cos^2\alpha + b^2\sin^2\alpha)} = \frac{3\mathrm{Ee_{max\,,i}}}{\mathrm{L}^2}\delta \tag{10}$$

Rearranging Equation 10, the yield displacement, $\delta_{yield,i}$, is obtained as a function of the yield stress, $\sigma_{yield,i}$:

$$\delta_{\mathrm{yield\,,i}} = \frac{\sigma_{\mathrm{yield\,,i}}\mathrm{L}^2}{3\mathrm{Ee_{max\,,i}}} \tag{11}$$

As can be inferred from Equation 11, the yield displacement, $\delta_{yield,i}$, of the cantilever member is inversely proportional to the maximum eccentricity, $e_{max,i}$, of the cross section. Therefore, as the deflection direction becomes increasingly oblique, the maximum eccentricity also increases, and so, the displacement at which the element first yields is reduced. The yield displacement is minimum when the deflection direction is at 45° as per Figure 17(c). This is consistent with the patterns observed in the safety envelopes. A point of minimum safe displacement is seen when the displacement direction is 45° about any principal axis.

The findings of the analytical model are consistent with the findings of Montesano and Singh [19] and Baptista [20] – stresses increase to a maximum when the biaxial stressing direction is half way between two principal axes, i.e. stresses in an element are inversely proportional to the maximum eccentricity of the member from its neutral axis. However, it is fair to assume the displacement values, and subsequent safety envelope, provide only a simple indication of the behaviour of the LSB to biaxial deformations. They may not be fully accurate and representative of the real-world safety envelope due to a number of potential sources of error as previously discussed in the Chapter 2. Similarly, the strain rate of the LSB model is not strictly representative of

real-world operating conditions. Large impact forces due to wheel-rail contact induce comparatively high-frequency displacements, and so the relatively slow deflection time of 6 seconds used in the model may influence the position at which the LSB first yields. The impact of strain rate on the mechanical properties of steel is well known; literature concerning this topic has concluded that a higher strain rate increases yield and tensile strength [22]. Based on these findings the ABAQUS model is likely to produce conservative results and hence a 'safer' safety envelope. Additionally, a higher deflection rate would have amplified the effect of inertial effects which are omitted from the analysis, as discussed in Chapter 2.

The LSB's geometry is much more complex than that of the representative element discussed above, and so, developing an analytical model for the LSB would be difficult; the FEA process has modelled and computed the response of the LSB. It is fair to assume the LSB behaves as a bar when deformed in the Left and Right directions, and as a beam when deformed Up, Down, Forward or Backward. A bar is a slender structural member which resists axial loads, and a beam is one which resists transverse loads and moments. The limits of the safety envelopes verify this reasoning – the weakest deflection directions are Left and Right (compression and tension respectively); a bar can resist small elongations and compressions before it reaches its yielding point, whereas a cantilever beam can be deflected transversely notably larger distances before yielding. Given the role of the LSB is primarily to resist lateral compressive and tensile forces (Left and Right) as it moves and restrains the switch blades, a higher sensitivity to yielding as seen in these directions is unwelcome.

The weakness seen in the Left and Right directions may be explained by the distribution of stresses within the LSB. The Left and Right directions show considerably higher stress levels throughout the LSB with a larger number of mesh elements having reached their yield stress (areas coloured grey in Figure 18) at the 50 mm deflection point. For all deflection directions, the highest stresses are seen, and the point of first yield is initiated, around the first bolt hole. The Up, Down, Left and Right deformations bend the LSB transversely only, this corresponds to high magnitude stresses appearing primarily at the first bolt hole. Conversely, the tensile and compressive deformations in the Left and Right directions induce internal axial stresses throughout the entire length of the LSB. This is in addition to large concentrations at the bend and at the bolt holes where both axial and bending stresses occur simultaneously. Figure 18 shows the distribution of stresses at 50 mm deflection for all uniaxial deformation directions and gives an indication of the magnitude of stresses in the LSB.

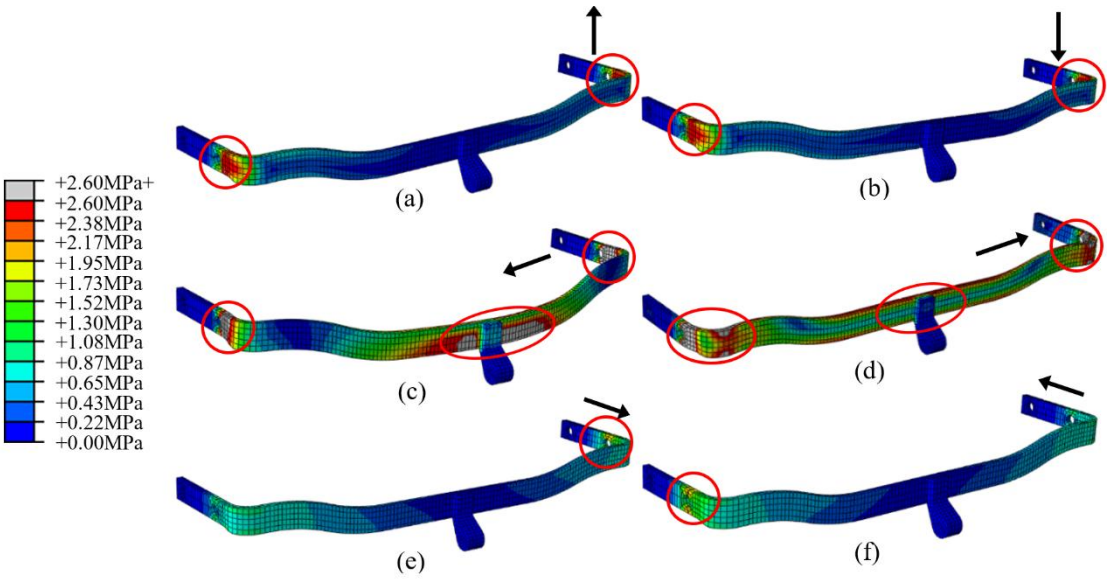

Figure 18. Von Mises stress distribution for uniaxial deformation directions, (a) Up, (b) Down, (c) Left, (d) Right, (e) Forward, (f) Back. Plastic stress areas circled red and elements coloured grey.

III. CONCLUSION

An investigation into a railway switch lock stretcher in which its biaxial behaviour was studied was carried out using the finite element analysis software ABAQUS. The FEM was validated against experimental data. One end of the LSB was fixed while the other was displaced until it started to plastically deform. A total of 62 displacement directions have been explored which collectively create a three-dimensional safety envelope showing the safe operating limits of the lock stretcher bar.

The performance of a lock stretcher bar is largely dependent on its ability to maintain a rigid shape throughout its lifetime, thus any scenarios which cause the LSB to deform plastically are dangerous. The findings suggest the biaxial failure characteristics of the LSB are a function of its geometry, and that the failure relationship previously assumed by Hemida et al. [9] as linear is incorrect. As the direction at which the LSB is

deformed becomes increasingly oblique, the permissible deflection reaches a sharp minimum when the deflection direction is at 45° about any principal axis. A representative analytical model has been created which rationalises the patterns observed in the data obtained; the maximum perpendicular eccentricity of a cross section about its neutral axis is inversely proportional to its yield displacement.

The findings of this study suggest the LSB is more sensitive to failure when exposed to biaxial deformations, particularly in the tensile and compressive (Left and Right) directions, than to pure uniaxial deformations, where it is least vulnerable. The permissible deformations of the LSB appear to be smaller than previously assumed for most deflection directions. Given the unlikelihood of the LSB deforming only in a uniaxial direction at any given time, the findings of this study suggest that the biaxial envelope would be a more appropriate criterion when specifying the suitability of a given LSB for its role in the switching panel.

REFERENCES

[1]. National Audit Office. A Short Guide to Network Rail, 1st ed. London: The Stationery Office; 2015.
[2]. Nicklisch D, Kassa E, Nielsen J, Ekh M, Iwnicki S. Geometry and stiffness optimization for switches and crossings, and simulation of material degradation. Proceedings of the Institution of Mechanical Engineers, Part F: Journal of Rail and Rapid Transit. 2010;224(4):279-292.
[3]. Rail Accident Investigation Branch (RAIB). Rail accident report: Derailment at Grayrigg 23 February 2007. Derby: Rail Accident Investigation Branch, Department for Transport; 2011.
[4]. HSE Potters Bar Investigation Board. Train derailment at Potters Bar 10 May 2002. Health and Safety Executive; 2013.
[5]. Rama D, Andrews J. A reliability analysis of railway switches. Proceedings of the Institution of Mechanical Engineers, Part F: Journal of Rail and Rapid Transit. 2013;227(4):344-363.
[6]. Aniołek K, Herian J. Numerical Modeling of Load and Stress on the Contact Surface of a Turnout and a Railway Vehicle. Journal of Transportation Engineering. 2013;139(5):533-539.
[7]. Snowdon J. Design Requirements for Street Track; Tramway Technical Guidance Note 1. London: Office of Rail Regulation; 2008.
[8]. Tomicic-Torlakovic M. Guidelines for the rail grade selection. Metalurgija. 2014;53(4):717-720.
[9]. Hemida H, Stewart E, Roberts C. Finite Element Analysis of the Lock Stretcher Bar in a Railway Switch. International Journal of Railway Technology. 2015;4(4):53-71.
[10]. Licciardello R, Bruner M, Corazza G, Cosciotti E, Malavasi G, Troisi R, Musella S. Some experience on the dynamics of turnouts due to passing trains. Seoul, South Korea: World Congress on Railway Research; 2008.
[11]. Ma J, Ma X, Zhou F, Ma H. An Approach to Track Maintenance Prioritization for Urban Rail Transit. Public Works Management & Policy. 2014;20(2):159-175.
[12]. Kassa E, Nielsen J. Dynamic interaction between train and railway turnout: full-scale field test and validation of simulation models. Vehicle System Dynamics. 2008;46(1):521-534.
[13]. Pålsson B, Nielsen J. Wheel–rail interaction and damage in switches and crossings. Vehicle System Dynamics. 2012;50(1):43-58.
[14]. Alfi S, Bruni S. Mathematical modelling of train–turnout interaction. Vehicle System Dynamics. 2009;47(5):551-574.
[15]. Pletz M, Daves W, Ossberger H. A wheel passing a crossing nose: Dynamic analysis under high axle loads using finite element modelling*. Proceedings of the Institution of Mechanical Engineers, Part F: Journal of Rail and Rapid Transit. 2012;226(6):603-611.
[16]. Eck S, Oßberger H, Oßberger U, Marsoner S, Ebner R. Comparison of the fatigue and impact fracture behaviour of five different steel grades used in the frog of a turnout. Proceedings of the Institution of Mechanical Engineers, Part F: Journal of Rail and Rapid Transit. 2013;228(6):603-610.
[17]. Zanenburg W. Degradation processes of switches & crossings. IET International Conference on Railway Condition Monitoring. 2006.
[18]. Li X, Nielsen J, Pålsson B. Simulation of track settlement in railway turnouts. Vehicle System Dynamics. 2014;52(1):421-439.
[19]. Montesano J, Singh C. Critical stiffness damage envelopes for multidirectional laminated structures under multiaxial loading conditions. Materials & Design. 2016;91:218-229.
[20]. Baptista A. Resistance of steel I-sections under axial force and biaxial bending. Journal of Constructional Steel Research. 2012;72:1-11.
[21]. Essa K, Hartley P. Numerical simulation of single and dual pass conventional spinning processes. International Journal of Material Forming. 2009;2(4):271-281.
[22]. Wiesner C, MacGillivray H. Loading Rate Effects on Tensile Properties and Fracture Toughness of Steel. 1999 TAGSI Seminar - 'Fracture, Plastic Flow and Structural Integrity'. Cambridge, UK; 1999.

Ludeen, W., Hemida, H. and Stewart, E. "Operating Limits of Railway Lock Stretcher Bar Movements via Multiaxial Analysis" The International Journal of Engineering and Science (IJES), 8.10 (2019): 01-14